Article

Influence of Common Assumptions Regarding Aerosol Composition and Mixing State on Predicted CCN Concentration

Manasi Mahish [1] iD, **Anne Jefferson** [2,3] **and Don R. Collins** [1],*

[1]   Department of Atmospheric Sciences, Texas A&M University, College Station, TX 77843, USA;
      manasi.mahish@gmail.com
[2]   Cooperative Institute for Research in Environmental Science (CIRES), University of Colorado,
      Boulder, CO 80309, USA; anne.jefferson@noaa.gov
[3]   NOAA Earth System Research Laboratory, Boulder, CO 80305, USA
*   Correspondence: dcollins@tamu.edu; Tel.: +1-979-862-4401

Abstract: A 4-year record of aerosol size and hygroscopic growth factor distributions measured at the Department of Energy's Southern Great Plains (SGP) site in Oklahoma, U.S. were used to estimate supersaturation (S)-dependent cloud condensation nuclei concentrations (N_{CCN}). Baseline or reference $N_{CCN}(S)$ spectra were estimated using κ-Köhler Theory without any averaging of the measured distributions by creating matrices of size- and hygroscopicity-dependent number concentration (N) and then integrating for S > critical supersaturation (S_c) calculated for the same size and hygroscopicity pairs. Those estimates were first compared with directly measured N_{CCN} at the same site. Subsequently, N_{CCN} was calculated using the same dataset but with an array of simplified treatments in which the aerosol was assumed to be either an internal or an external mixture and the hygroscopicity either assumed or based on averages derived from the growth factor distributions. The CCN spectra calculated using the simplified treatments were compared with those calculated using the baseline approach to evaluate the error introduced with commonly used approximations.

---

1. Introduction

Indirect forcing by aerosols involves complex interactions between the aerosol and clouds that affect the droplet number concentration, albedo, precipitation efficiency, and lifetime of clouds and the chemical processing and scavenging of aerosol particles. Mediating this interaction are cloud condensation nuclei (CCN), which are those particles that activate to form droplets at a given supersaturation (S), known as the critical supersaturation (S_c). In part because of the high temporal and spatial variability of aerosol and clouds, climate model predictions of indirect forcing have a high uncertainty. Estimates of CCN concentration (N_{CCN}) using detailed size-dependent aerosol chemical composition are computationally intensive and simplifications used to minimize computation introduce additional uncertainty.

Methods of determining aerosol activation have evolved to consider complex aerosol composition and structure. Particle S_c can be determined for inorganic species using Köhler Theory, provided the physico-chemical properties of the solutes are known [1]. However, atmospheric aerosols frequently contain a significant amount of organic material as well [2,3]. Compared with soluble inorganic particles, those composed entirely of organic species have higher S_c and are often comparatively inefficient in droplet formation [4,5]. But the solubility and surface tension-reducing properties of the organic component can sometimes have significant influence on S_c [6–13]. Extended Köhler Theory can

predict CCN concentration of a multi-component aerosol reasonably well from a description of its size distribution and chemical composition [9,10,14–16]. Introduction of a single hygroscopicity parameter by Petters and Kreidenweis [17] has simplified description and comparison of hygroscopicity and CCN activity for particles composed of single or multiple inorganic and organic species [18].

CCN concentration is also dependent upon aerosol mixing state. Previous closure studies have shown that assumption of an internal mixture generally results in an overestimate of the CCN concentration and assumption of an external mixture in an underestimate [19–34]. However, assumption of either mixing state leads to reasonable results for aged aerosols [35]. While inclusion of mixing state [36–40] and chemical composition [37,38,41–44] can increase the accuracy with which CCN concentration can be estimated, both can be highly variable with time and with particle size, and are often unavailable with current measurement techniques and not easily incorporated into aerosol descriptions used in models. Moreover, chemical composition and mixing state are greatly simplified in large scale models, with simple categorizations such as inorganic/organic and internal/external mixture. Supporting such treatment, several studies have shown that N_{CCN} is most sensitive to the aerosol size distribution [45,46], and the assumption of internal mixing has resulted in fairly accurate predictions [42,47–52]. Ervens et al. [35,53] reported that description of the mixing state is relatively more important than that of the size-resolved chemical composition. Other studies suggest detailed information of size distribution, chemical composition, and mixing state is important for achieving closure among aerosol and CCN measurements [38,43,44,54–58].

Here we use size-resolved aerosol concentration and subsaturated hygroscopicity measurements to estimate CCN concentration using an array of assumptions for composition and mixing state. The data were collected by the U.S. Department of Energy's (DOE) Atmospheric Radiation Measurement (ARM) program at the Southern Great Plains (SGP) site in rural Oklahoma. The study evaluates N_{CCN} estimation methods of varying degrees of complexity with respect to size, chemical composition, and mixing state. Baseline CCN spectra (N_{CCN} vs. S) were first derived by using (i) each combined set of size and hygroscopicity distributions and (ii) κ-Köhler Theory to create pairs of matrices describing (i) N and (ii) S_c, respectively, as a function of particle dry diameter, D_d, and hygroscopic growth factor, GF. The N_{CCN}(S) for each measurement set was calculated by integrating the N matrix over all elements for which $S > S_c$. Those results were compared with direct measurements of N_{CCN} made at the site to confirm that the calculated spectra were reasonably accurate. The objective was not to perform a rigorous closure analysis with consideration of measurement uncertainties but rather to simply evaluate the consistency of the datasets. Spectra calculated using a number of alternate approaches and assumptions were then compared to those from the baseline approach and the results were used to consider the scatter and bias introduced with simplifications commonly employed in large scale models.

2. Experiments

2.1. Site Description and Measurements

The data were recorded at the Southern Great Plains (SGP) central facility (CF1) (36°36′18.0″ N, 97°29′6.0″ W), located in a mixed land use area of cattle pastures and agricultural fields (mainly wheat, hay and corn) near Lamont, OK, USA. The climate at the site is continental with hot and humid summers and cool winters. The site is impacted by air masses originating from several regions, with accompanying diversity in aerosol concentration and properties. The chemical composition of the aerosol found at the site is complex and highly variable with time (evident in Figures S1 and S2) and with particle size. The size dependence of aerosol composition as reflected in that of GF was described by Mahish and Collins [59]. Table 1 lists the routine aerosol measurements at the site that were used for the analysis presented here. All datasets used for this analysis are available for download from the ARM archive. Data from the scanning mobility particle sizer (SMPS)/hygroscopicity tandem differential mobility analyzer (HTDMA) system were used for most of the analyses described here.

That instrument sequentially measures a size distribution and then a set of hygroscopic growth factor distributions at 7 dry particle sizes every ~45 min. Nafion tube bundles are used to dry the sample flow prior to entering the upstream DMA and to humidify it to 90% RH between the two DMAs when measuring hygroscopicity. The sheath and excess flows are recirculated using a variable speed blower. The sample flow rate is controlled by varying the amount of dilution flow that is introduced upstream of the 3.0 L min^{-1} TSI 3762 condensation particle counter (CPC). Details of the SMPS/HTDMA system and processing of the data it generates are available in the Tandem Differential Mobility Analyzer/Aerodynamic Particle Sizer handbook posted on the ARM archive site [60] and in the work of Gasparini et al. [61]. As noted above, the calculated CCN spectra were compared with direct measurements at the site made with a DMT CCN-100 counter (CCNc) [62]. The CCNc cycles through 7 fixed supersaturations every half hour. A description of the instrument and data processing is available in the Aerosol Observing System (AOS) handbook [63]. Non-refractory chemical composition and black carbon content measured with an Aerosol Chemical Speciation Monitor [64] and a Particle Soot Absorption Photometer [65] were used in the selection of a representative hygroscopicity of the organic component for use in some of the calculations. Details of those instruments are available in the ACSM [66] and AOS [63] handbooks.

Table 1. List of instruments, measured quantities, manufacturer, and year installed.

Instrument	Measurement	Manufacturer/Model	Installation Date
Scanning Mobility Particle Sizer (SMPS; part of the "TDMA" system)	Size distribution from 0.012 to 0.74 μm dry diameter (D_d)	Fabricated, Texas A&M University, TX, U.S.	2005
Hygroscopic Tandem Differential Mobility Analyzer (HTDMA; part of the "TDMA" system)	Hygroscopic growth factor distributions of 0.013, 0.025, 0.05, 0.1, 0.2, 0.4, and 0.6μm D_d particles at 90% RH	Fabricated, Texas A&M University, TX, U.S.	2005
Cloud Condensation Nuclei counter (CCNc)	CCN concentration at a fixed set of supersaturations	CCN-100 Droplet Measurement Technologies, Longmont, CO, U.S.	2009
Condensation Particle Counter (CPC)	Concentration of D_d > 0.01 μm particles	Model 3010 TSI, Inc., Shoreview, MN, U.S.	1996
Aerosol Chemical Speciation Monitor (ACSM)	Sub 1-μm chemical composition (organics, sulfate, nitrate, ammonium, and chloride)	Aerodyne Research, Inc., Billerica, MA, U.S.	2010
Particle Soot Absorption Photometer (PSAP)	Sub 1-μm absorption coefficient (used to infer black carbon concentration)	Radiance Research, Seattle, WA, U.S.	1992

2.2. Screening and Time Interval Selection

Data from each instrument were validated separately and periods having erroneous data or no data were excluded from analysis. Data from time periods during which instrument problems or failure was evident or when one of the following occurred were not used:

a.   The total particle concentration (N_{CN}) calculated by integrating the SMPS size distribution differed significantly from that directly measured with the CPC

b.   The N_{CCN} measured with the CCNc exceeded the N_{CN} measured by the CPC, possibly due to malfunction of the CCNc

c.   The sample flow entering the upstream (1st) DMA had an RH > 30%, or

d.   The sample flow entering the downstream (2nd) DMA had an RH < 85%.

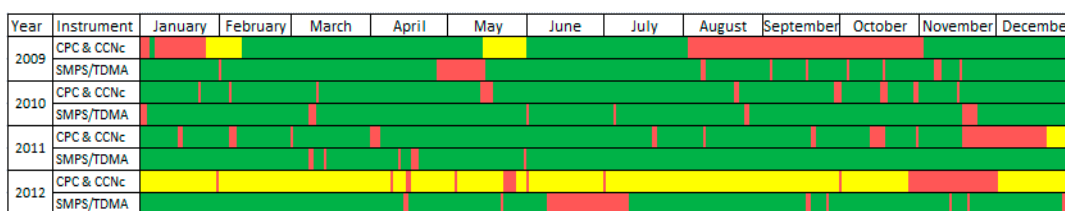The categorized data quality during the period of analysis is shown in Figure 1.

Figure 1. Data quality during the analysis period. Periods during which data are available and no significant problems were identified are colored green, those during which confidence in at least some subset of the data is low are yellow, and those during which data are unavailable or thought to be erroneous are red. Data used to generate this graph are available at the site identified in the Acknowledgments section below.

2.3. Use of K-Köhler Theory

For each of the approaches used to estimate N_{CCN}, the calculation of S_c from measured particle size and measured or assumed hygroscopicity employed κ-Köhler Theory [17]. The κ values of aerosol constituents were assumed to be the same in the aqueous particles as measured in the HTDMA at 90% RH and in the more dilute solutions at the point of activation to form cloud droplets. This has the same effect as assuming that the water activity coefficient in the solutions is constant and that all soluble species are fully dissolved at the RH in the HTMDA. A more accurate treatment for which activity coefficients or κ are calculated as a function of RH (and solution concentration) is not justified because size-resolved composition measurements are not available and the bulk submicron measurements made with the ACSM show the aerosol composition is complex and varies considerably during the year. Specifically, there is a strong seasonality in the soluble inorganic content, with sulfate dominant from roughly April through October and nitrate dominant from November through March, as is evident in the sulfate:nitrate ratio shown in Figure 2. Thus, the choice of soluble inorganic component(s) needed to model the extent and effect of variation in κ between 90% RH and at S_c would vary by month over the 4-year period of this analysis, as well as over shorter periods of days or even hours accompanying changes in the origin and processing of the sampled aerosol. Furthermore, any attempt to estimate RH-dependent changes in κ would require consideration of the influence of the significant organic content at the site. As shown in Table 2, averaged throughout the year organics contribute over 50% to the total submicron mass concentration.

Table 2. Mass concentration fraction from ACSM measurements at SGP.

Year	Mass Concentration Fraction (%)		
	Total Organics	Ammonium Sulfate	Ammonium Nitrate
2011	57	17	26
2012	56	18	26
2013	56	24	20

For all CCN concentration estimate approaches for which the HTDMA data were used, GF was related to κ using the following expression from Petters and Kreidenweis [17].

$$\kappa = \left([GF(RH)]^3 - 1\right) \frac{\left(\exp\left(\frac{A}{GF(RH) \cdot D_d}\right) - RH\right)}{RH}$$
$$A = \frac{4 \cdot \sigma_{sol} \cdot M_w}{R \cdot T \cdot \rho_w} \tag{1}$$

where M_w and ρ_w are the molecular weight and liquid density of water, respectively. The solution surface tension, σ_{sol}, was assumed to be that of pure water, 0.072 J m^{-2}. Because it is assumed that κ values were the same for the more concentrated and the more dilute aqueous solutions in the HTDMA and at activation, respectively, it is not necessary to know the contributions of different

aerosol components to the overall hygroscopicity for the internal mixture calculations. But for assumed external mixtures the hygroscopicity of two or more particle types must be determined or assumed. For this analysis, particle types assumed to be present in external mixtures were (i) particles composed of soluble inorganics; (ii) particles composed of soluble organics; and (iii) particles composed of insoluble (and non-hygroscopic) components. The hygroscopicity parameter of the soluble inorganic particles, κ_{inorg}, was assumed to be 0.6, which is similar to that of ammonium sulfate and ammonium nitrate. As aerosol organic components at the SGP site are not well characterized, direct derivation of κ_{org} is not possible. Here, κ_{org} was estimated using the mixing rule [17].

$$\kappa_{org} = \frac{V_{overall}\kappa_{overall} - \left\{ V_{overall} - \left(\frac{m_{orgNR}}{\rho_{orgNR}} + \frac{\frac{b_{absBC}}{\beta_{BC}}}{\rho_{BC}} \right) \right\} \kappa_{inorg}}{\frac{m_{orgNR}}{\rho_{orgNR}}} \qquad (2)$$
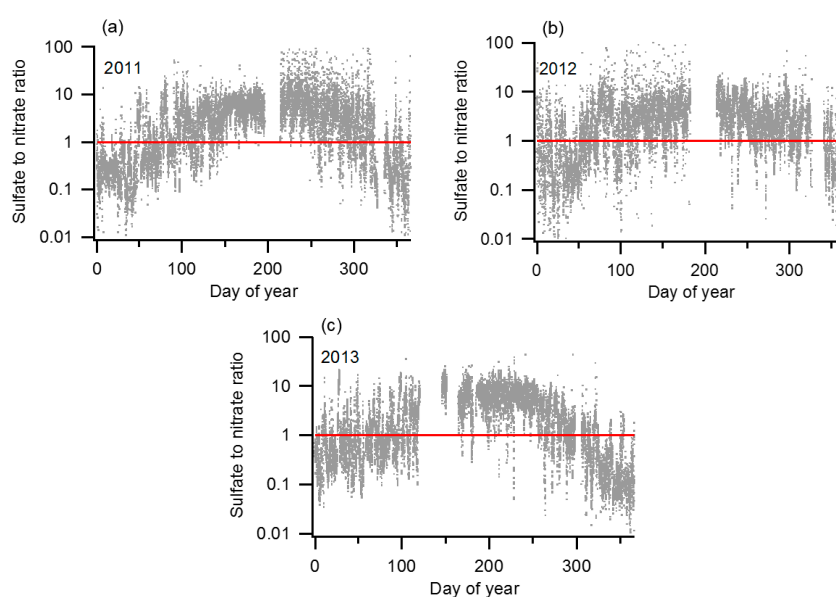

Figure 2. Sulfate to nitrate equivalent concentration ratio based on ACSM chemical composition data from (**a**) 2011, (**b**) 2012, and (**c**) 2013. Equivalent concentration = $\frac{molar\ concentration}{equivalence\ factor}$, where the equivalence factor for sulfate and nitrate are 0.5 and 1, respectively.

For these calculations the total particle volume concentration ($V_{overall}$) was determined from the measured size distribution. The submicron average hygroscopicity parameter ($\kappa_{overall}$) was calculated from the measured size and hygroscopicity distributions as the volume concentration-weighted average κ. The mass concentration of non-refractory organics (m_{orgNR}) was measured by the ACSM and that of black carbon, BC, was estimated as the ratio of measured submicron particle light absorbance (b_{absBC}) and an assumed absorption efficiency at 0.55 μm wavelength of 7.5 $m^2\ g^{-1}$ [67]. The density, ρ, of non-refractory organics and BC were both assumed to be 1.3 g cm^{-3} [68].

The resulting seasonal profiles of $\kappa_{overall}$ and κ_{org} in 2011 are shown in Figure 3. Unlike the κ_{org} profile, $\kappa_{overall}$ was highest in the winter and lowest in the summer. The high wintertime $\kappa_{overall}$ is a result of high concentrations of inorganic compounds, especially nitrate, while the relatively low summertime $\kappa_{overall}$ is caused by higher organic mass concentrations, as shown in Figure 4. Positive Matrix Factorization (PMF) analysis used for the Organic Aerosol Component (OACOMP) ARM Value Added Product (VAP) [69] indicates that less-hygroscopic biomass burning organic aerosol (BBOA) was prevalent from February through April in 2011, thus lowering κ_{org} in winter and spring. Aged SOA (MO-OOA), which is moderately hygroscopic, was more abundant in summer, and thus

raised κ_{org}. The κ_{org} in the spring and fall lies between that of the winter and summer. The 2011 average of 0.1 was used for this study, while the sensitivity of the results to the selected value was assessed by repeating the calculations for the seasonal minimum (κ_{org} = 0.06, winter) and maximum (κ_{org} = 0.16, summer).
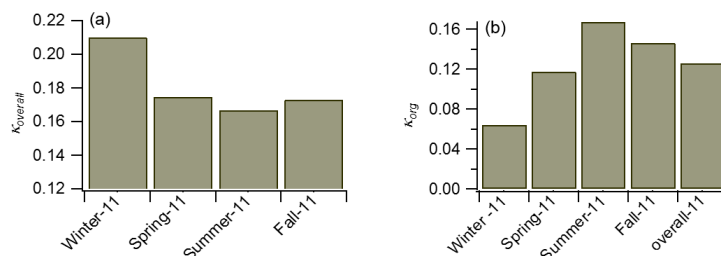

Figure 3. Seasonal profile of (**a**) $\kappa_{\mathrm{overall}}$ (left) and (**b**) κ_{org} (right) in 2011.
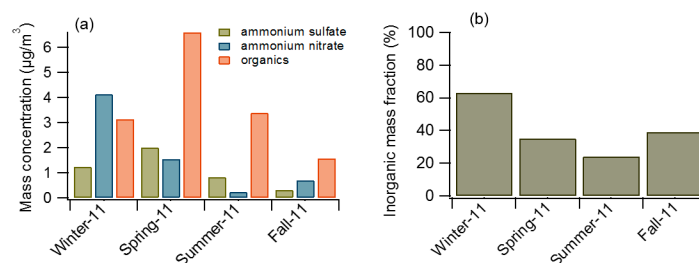

Figure 4. Seasonal average of (**a**) organic and inorganic mass concentration and (**b**) the inorganic mass fraction (%) in 2011.

2.4. Description of Models Used for Estimating N_{CCN}

To simplify both the comparison of the varied approaches used to estimate N_{CCN} and the comparison of the results, a common framework will be used to describe all of the approaches even though more straightforward descriptions would suffice for many of them. For all approaches a CCN spectrum, $N_{CCN}(S)$, was calculated for each size distribution measured by the SMPS. For the simplest approaches, the HTDMA data were not considered and a fixed hygroscopicity parameter was assumed. For all others the GF distributions were interpolated and extrapolated to each of the 90 size bins in the size distribution measurements and then converted to κ distributions using Equation (1). The differences among the approaches arise from the use and (any) averaging of the κ distributions, as summarized in Figure 5.
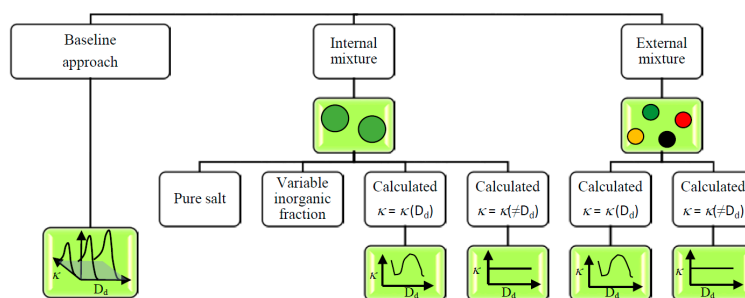

Figure 5. Overview of the N_{CCN} calculation approaches.

As a baseline for comparison with estimates from other approaches and with direct measurements, N_{CCN} was calculated using the full GF distributions without any averaging. Because all of the

information in the GF distributions is retained, these estimates are expected to be more accurate than those from any of the other approaches, all of which rely on averaged or assumed hygroscopicity. For each measurement sequence the interpolated κ distributions were combined with the size distribution to create a matrix of number concentrations as a function of D_d and κ, such as that shown graphically in Figure 6a. A Köhler curve relating equilibrium S to droplet diameter, D, was calculated for each (D_d, κ) pair using Equation (3) below. The S_c for each pair was calculated as the maximum value of equilibrium S along the curve.

$$S(D) = \frac{D^3 - D_d^3}{D^3 - D_d^3(1 - \kappa)} \exp\left[\frac{4M_w \sigma_{sol}}{RT\rho_w D}\right] - 1 \tag{3}$$

As with calculations using Equation (1), σ_{sol} was assumed to be that of water, 0.072 J m^{-2}. The result can be viewed as a matrix with elements of S_c and the same D_d and κ arrays as used in the number concentration matrix described above. N_{CCN} was estimated for a prescribed S by integrating the number concentration $N(D_d, \kappa)$ for which $S > S_c$. This is presented graphically in Figure 6b, with N_{CCN} calculated by summing the N elements (whole or part) above and to the right of one of the four curves, each of which connects the elements having the same S_c. The resulting N_{CCN} estimates were first compared with direct measurements made with the CCNc and then with the results of the other estimate approaches outlined below.

For all other N_{CCN} estimates the aerosol was assumed to be either an internal mixture or an external mixture, as is generally required for regional and global scale climate models. The goals here were to assess the error introduced when making these simplifying assumptions and to identify the approach(es) most suitable for an aerosol similar to that found at SGP.

To treat the aerosol as an internal mixture the D_d-dependent κ distributions described above were replaced with a single κ value that is either dependent on D_d ($\kappa = \kappa(D_d)$) or the same for all D_d ($\kappa \neq \kappa(D_d)$). The former comes simply from the number concentration-weighted average of the κ distributions at each D_d, with the result depicted in Figure 6c in the same manner as for the baseline approach matrix. For approaches for which κ is assumed to be size independent, it was calculated either as the average of $\kappa(D_d)$ (Figure 6d) or, neglecting the hygroscopicity measurements, as that of particles composed of 20%, 50%, or pure soluble inorganics (~ammonium sulfate, AS) by volume ($\kappa = 0.12, 0.30$, and 0.60, respectively, with only $\kappa = 0.30$ shown in Figure 6g for clarity).

External mixtures were assumed to be comprised of two of the three particle types considered: insoluble, $\kappa = 0.0$, organic, $\kappa_{org} = 0.1$, and inorganic, $\kappa_{inorg} = 0.6$. As with the assumed internal mixture approaches, both size dependent and size independent scenarios were considered. For both, independent size distributions of the different particle types were calculated from the average $\kappa(= f(D_d)$ or $\neq f(D_d))$ using Equations (4) and (5) below.

Case 1: for $\kappa(D_d) > \kappa_{org}$

$$\begin{gathered} \left(\frac{dN}{d\log D_d}\right)_{inorg} = \frac{\kappa(D_d) - \kappa_{org}}{\kappa_{inorg} - \kappa_{org}}\left(\frac{dN}{d\log D_d}\right)_{SMPS} \\ \left(\frac{dN}{d\log D_d}\right)_{org} = \left(\frac{dN}{d\log D_d}\right)_{SMPS} - \left(\frac{dN}{d\log D_d}\right)_{inorg} \\ \left(\frac{dN}{d\log D_d}\right)_{insoluble} = 0 \end{gathered} \tag{4}$$

Case 2: for $\kappa(D_d) \leq \kappa_{org}$

$$\begin{gathered} \left(\frac{dN}{d\log D_d}\right)_{org} = \frac{\kappa(D_d)}{\kappa_{org}}\left(\frac{dN}{d\log D_d}\right)_{SMPS} \\ \left(\frac{dN}{d\log D_d}\right)_{insoluble} = \left(\frac{dN}{d\log D_d}\right)_{SMPS} - \left(\frac{dN}{d\log D_d}\right)_{org} \\ \left(\frac{dN}{d\log D_d}\right)_{inorg} = 0 \end{gathered} \tag{5}$$

The results for $\kappa(D_d)$ and $\kappa(\neq D_d)$ are depicted graphically in Figure 6e,f, respectively, where the lower and higher horizontal lines represent the organic and inorganic particle types, respectively. As with the other approaches, N_{CCN} was calculated by summing N elements above and to the right of the constant S_c curves. Contributions from the inorganic and organic particle types can also be calculated separately and then added to determine the total N_{CCN} (i.e., $N_{CCN} = N_{CCN.inorg} + N_{CCN.org}$).
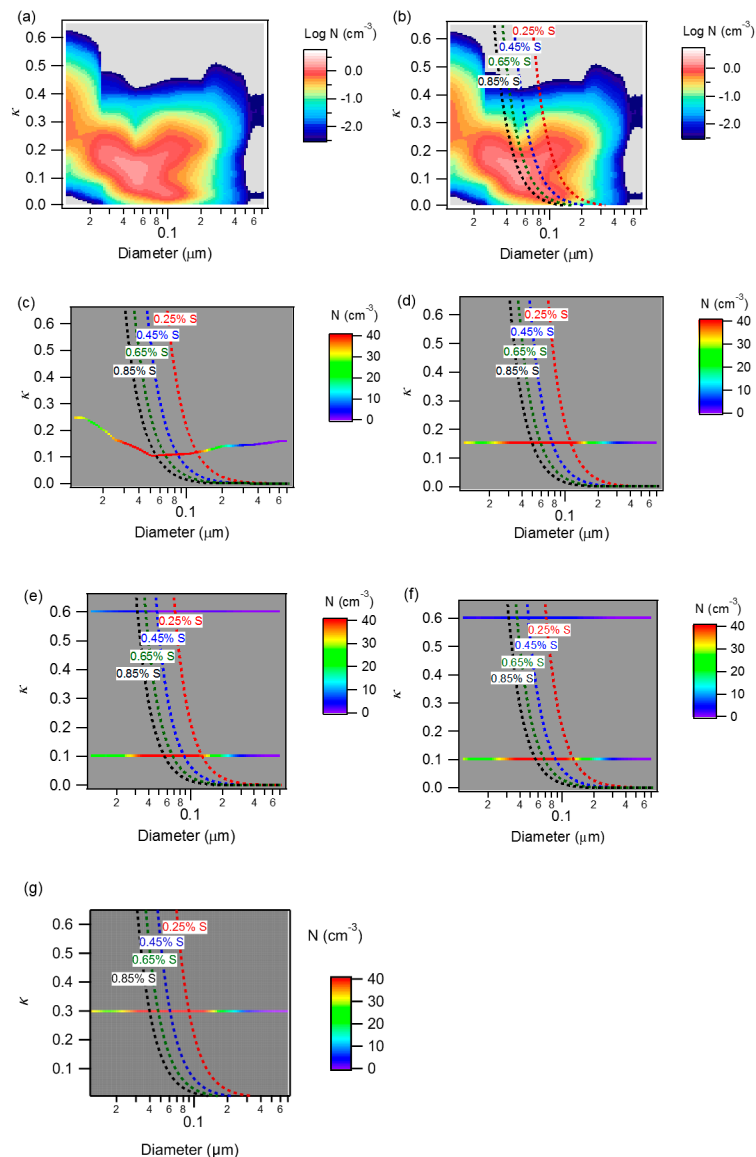

Figure 6. A graphical illustration of the approaches used to estimate N_{CCN}. (**a**) Number concentration matrix calculated from a set of measured size and GF distributions. The size distribution is partitioned among the κ bins according to the GF distributions interpolated to each D_p without any averaging or assumptions about mixing state or composition. The same matrix is shown in (**b**); with lines of constant S_c added. As with all of the estimation techniques, $N_{CCN}(S)$ is estimated by summing the concentration elements (whole or part) above and to the right of the constant S_c (= S) lines; The graphs in (**c**–**g**) are from the same set of size and GF distributions as those used for (**a**,**b**); but with various assumptions for mixing state and composition that collapse the κ distribution at each bin in the size distribution to one or two values; (**c**) internal mixture with $\kappa(D_d)$; (**d**) internal mixture with $\kappa(\neq D_d)$; (**e**) external mixture with $\kappa(D_d)$; (**f**) external mixture with $\kappa(\neq D_d)$; and (**g**) internal mixture with an assumed inorganic volume fraction of 0.5.

3. Results and Discussion

3.1. Comparison between Measured and Baseline N_{CCN} Estimate

The concentration measured by the CCNc was compared to that calculated using the baseline approach for all available data from 2009–2012. The results for May 2011 are shown in Figure 7 and for all of 2011 in Figure S3.
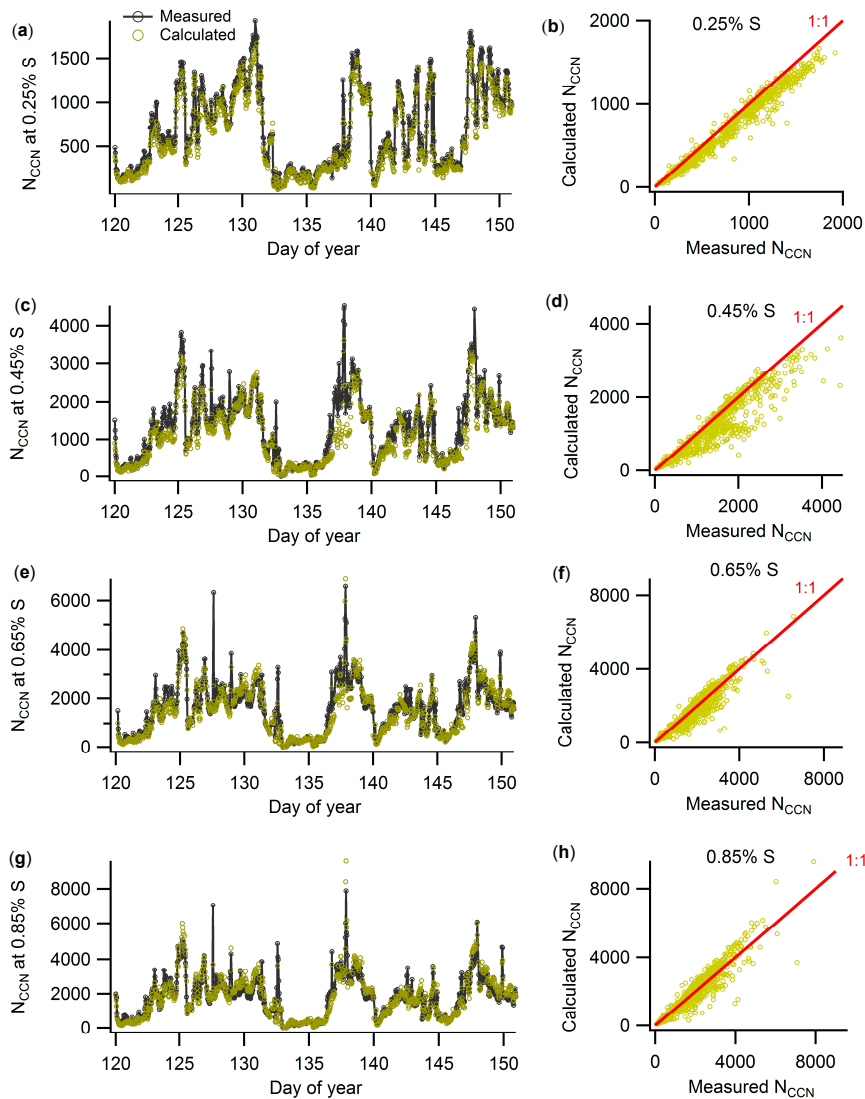

Figure 7. Comparison between measured and estimated N_{CCN} (cm^{-3}) for May 2011 at 0.25% (**a**,**b**); 0.45% (**c**,**d**); 0.65% (**e**,**f**); and 0.85% S (**g**,**h**). The dotted lines in the scatter plots represent $+/- 20\%$ relative to the 1:1 line.

The calculated N_{CCN} tracks that measured throughout the period considered. The deviation between the two is quantified as the Normalized Root Mean Square Error (NRMSE)

$$\text{NRMSE} = \left\{ \frac{1}{n} \sum_{i=0}^{n-1} \left(\frac{x_i - y_i}{x_i} \right)^2 \right\}^{0.5} \tag{6}$$

where x_i is the measured N_{CCN} at a given S, y_i the estimated N_{CCN} at the same S, and n the number of concentration pairs compared. The average NRMSE between the measured and calculated

concentrations for May 2011 and for each of the four years analyzed are summarized in Table 3. The measured N_{CCN} at 0.25% S during 2012 was very noisy and was excluded from the analysis.

Table 3. NRMSE between measured and estimated N_{CCN} at 4 different S from 2009–2012 and for May 2011.

Year/Month	NRMSE @ % S			
	0.25	0.45	0.65	0.85
2009	0.53	0.36	0.35	0.35
2010	0.22	0.29	0.27	0.25
May 2011	**0.17**	**0.22**	**0.21**	**0.21**
2011	0.29	0.29	0.26	0.26
2012	-	0.33	0.38	0.36

In addition to measurement error, some possible reasons for deviations between the measured and calculated concentrations are (i) differences in assumed and actual properties of aerosol chemical species; (ii) interactions among components not captured by κ-Köhler Theory; (iii) the presence of low solubility organics that dissolve under the dilute conditions with S ~S_c but not in the more concentrated solution in the HTDMA at 90% RH; (iv) the presence of particles that contain slowly dissolving compounds or that are in an amorphous/glassy state for which hygroscopic growth and activation timescales may be comparable to or greater than the HTDMA and CCNc residence times; and (v) the presence of surface tension-reducing species, which influence S_c much more than GF. But as noted above, the primary goal here was not to assess closure but to confirm that the baseline spectra calculated from the size and GF distributions were reasonably accurate and were suitable to serve as the reference for comparison with the results from the simplified treatments of composition and mixing state.

3.2. Comparison of N_{CCN} Calculated from Different Approaches

Estimates of N_{CCN} assuming the aerosol is an internal or external mixture relative to those of the baseline approach for which no assumption about mixing state is made are presented in Figures 8 and 9 for 0.25% and 0.85%, respectively, and in Figures S4 and S5 for 0.45% and 0.65% S, respectively. Deviations from the 1:1 lines are interpreted as error introduced by the averaging or approximations required for all but the baseline calculations. Best fits through the data were assumed to be linear and were forced through the origin to facilitate interpretation of the results and simply because of the apparent linear correlations with minimal offset in the figures. Table 4 summarizes the slope ($m = \frac{N_{CCN} \text{ from alternate approach}}{N_{CCN} \text{ from baseline approach}}$) and goodness of fit ($r^2$) for each of the approaches with respect to the baseline estimate. Values of m above (below) 1 indicate that the simplified treatment results in N_{CCN} greater (less) than that from the baseline estimate for a given S. Treating the aerosol as an internal mixture with size dependent hygroscopicity resulted in the best agreement with the baseline estimates, with the average m closest to 1.0 and the highest r^2 (Table 4). Though there is considerably more scatter in the results for the internal and external mixtures with $\kappa(\neq D_d)$ than in those with $\kappa(D_d)$, the deviations are found to be tightly correlated. The relationships between the results for the assumed internal and external mixtures with $\kappa(\neq D_d)$ are shown in Figure 10e,f. The strong correlation in $N_{CCN}(S)$ obtained for those assumed internal and external mixtures could be interpreted as reflecting a general lack of sensitivity to the mixing state as has been reported in some closure studies. But, at least for these data, both estimates simply differ in the same direction from what is believed to be the most accurate estimate. For both mixing state assumptions, the estimated N_{CCN} with $\kappa(\neq D_d)$ is higher than that with $\kappa(D_d)$, as the κ averaged over the complete size range is typically higher than the $\kappa(D)$ over the ~0.05–0.20 µm size range that dominates N_{CCN}.
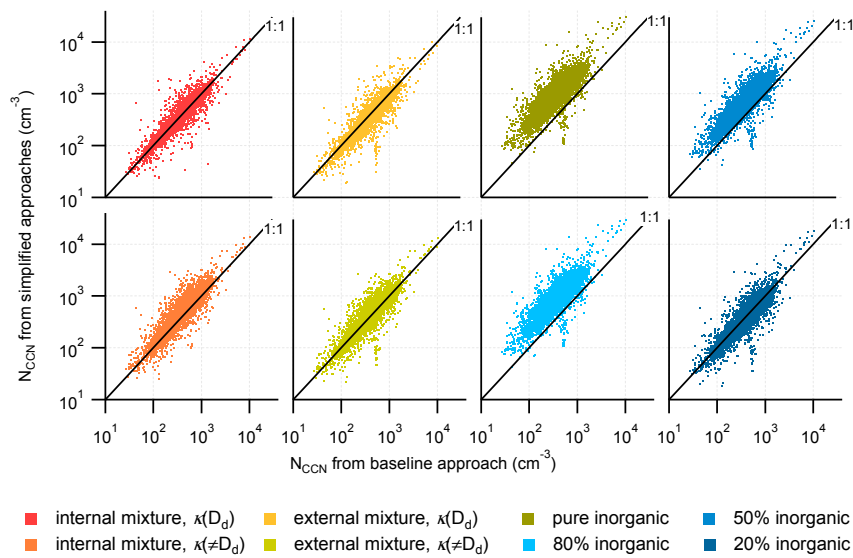
Figure 8. N_{CCN} estimated from simplified approaches vs. that from the baseline approach at 0.25% S for all 2011 data.
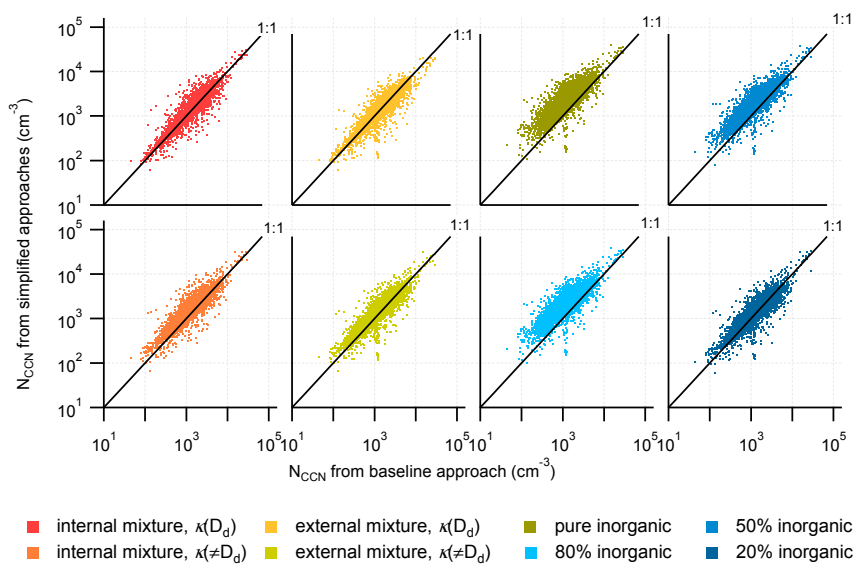

Figure 9. N_{CCN} estimated from simplified approaches vs. that from the baseline approach at 0.85% S for all 2011 data.

Table 4. Fit parameters of N_{CCN} estimate approaches for 2011 data

Model	Slope (*m*) @ % S				$\dfrac{m_{0.25\% \ S} - m_{0.85\% \ S}}{m_{0.25\% \ S}}$	Correlation Coefficient (r^2) @ % S			
	0.25	0.45	0.65	0.85		0.25	0.45	0.65	0.85
Baseline	1	1	1	1	0	1	1	1	1
Internal, $\kappa = \kappa(D_d)$	1.01	1.02	1.01	1.01	0.002	0.87	0.87	0.85	0.84
Internal, $\kappa = \kappa(\neq D_d)$	1.21	1.18	1.13	1.10	0.095	0.82	0.81	0.80	0.80
External, $\kappa = \kappa(D_d)$	0.90	0.92	0.90	0.90	0.009	0.81	0.81	0.78	0.77
External, $\kappa = \kappa(\neq D_d)$	1.06	1.07	1.02	1.00	0.061	0.80	0.80	0.79	0.77
Internal, pure AS	2.37	1.82	1.57	1.43	0.400	0.67	0.69	0.68	0.67
Internal, 50% AS	1.76	1.50	1.33	1.26	0.285	0.72	0.75	0.76	0.74
Internal, 20% AS	1.05	1.05	1.03	0.99	0.057	0.72	0.78	0.77	0.76

A correction of $1/m$ could be applied to results using any of the simplified treatments to increase accuracy. Of course, that sort of annual average correction would not reduce error that arises from variability in aerosol characteristics on seasonal or shorter time scales and is reflected in the r^2 values. For example, assuming the aerosol has a fixed κ of 0.12 (20% AS) results in average best fit slopes between 1.00 and 1.06, indicating that, on average, an error of only a few percent would be introduced if both the composition and hygroscopicity were not considered at all in the calculations. However, that represents the average of comparably large negative and positive errors for individual measurements or days, as is shown in Figure 11 that compares the 2011 daily averages of the results from the internal mixture with $\kappa(D_d)$ and the fixed 20% AS treatments relative to the baseline calculations. And as is shown in Figure 10, similar deviations from the 1.0 line are evident in the results for which the hygroscopicity was considered, but not its size dependence. Furthermore, the utility of any of the simplifying approaches is limited if not applicable over a wide range in S. The S dependence of the best fit slopes quantified as the fractional change over the full range in S considered is included in the 6th column in Table 4. That S dependence is much lower for the two cases for which the size dependence of κ is considered than for any of the others, which is expected because the change in N_{CCN} with S largely reflects inclusion or exclusion of particles within a rather narrow slice of the full size range.
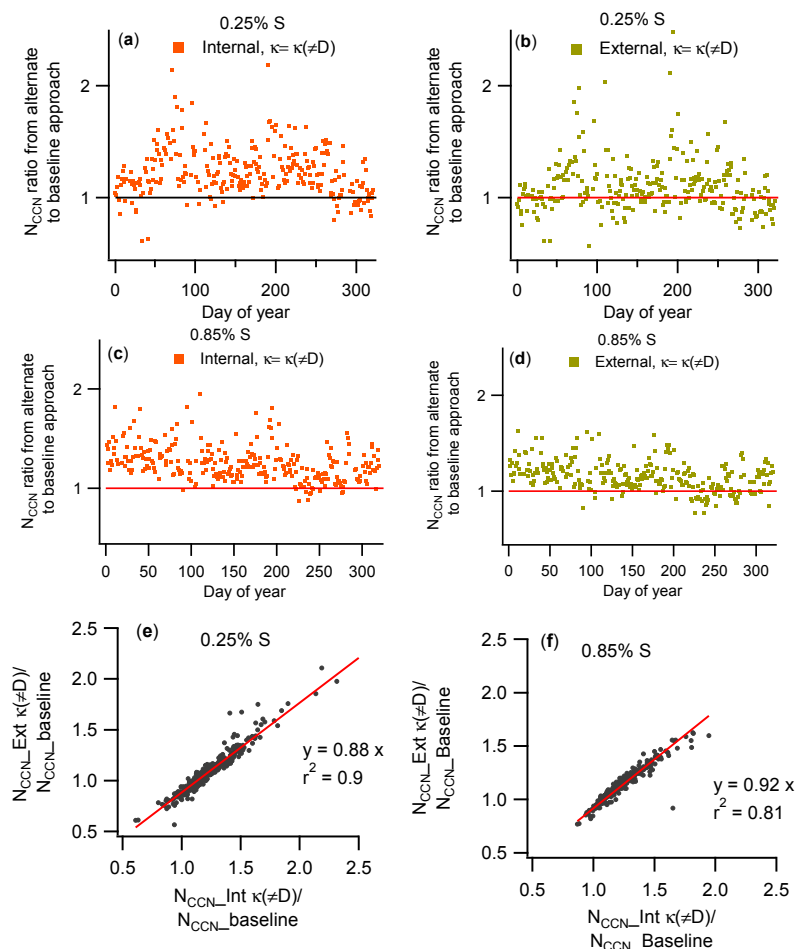

Figure 10. (**a**–**d**) Time series for 2011 of estimated N_{CCN} relative to that from the baseline approach: (**a**) internal mixture, $\kappa \neq \kappa(D)$ at 0.25% S; (**b**) external mixture, $\kappa \neq \kappa(D)$ at 0.25% S (**c**) internal mixture, $\kappa \neq \kappa(D)$ at 0.85% S; and (**d**) external mixture, $\kappa \neq \kappa(D)$ at 0.85% S; (**e**) Scatter plot of N_{CCN} ratio from (**a**,**b**); (**f**) scatter plot of N_{CCN} ratio from (**c**,**d**).

The results for the assumed external mixtures were found to be quite sensitive to the κ_{org} used. Specifically, substituting the seasonal minimum (0.06) for the annual average (0.10) of the estimated κ_{org} results in an average decrease in N_{CCN} of 8% when the size dependence of κ is considered and an increase of 10% when it is not. Similarly, use of the seasonal maximum of 0.16 results in an average decrease of 1% with $\kappa(D_d)$ and increase of 15% with $\kappa(\neq D_d)$. (The results for SGP are likely especially sensitive to the assumed value because it is similar to that average κ of 0.12 that was found to result in reasonable estimates averaged throughout the year). For any measurement a change in κ_{org} will cause a change in partitioning between the three particle types, with the net influence on N_{CCN} depending on the coupling of that change and the shape of the size distribution. Because the approach used allows for at most two particle types, an increase in κ_{org} that crosses the average κ of the aerosol will cause a shift in the assumed mixture from consisting of organic and inorganic ($\kappa = 0.6$) particles to organic and insoluble ($\kappa = 0.0$) particles, with a resulting increase in N_{CCN} due to the increased hygroscopicity of the organic particles, a decrease due to the loss of the inorganic particles, and a net change that could be positive or negative. To evaluate the sensitivity of the calculated N_{CCN} to the choice in κ_{inorg}, the analysis was repeated using values of 0.64 and 0.67 (instead of 0.6). The average change in N_{CCN} was about 0.6% when size-dependence is considered and about 1.0% when it is not.
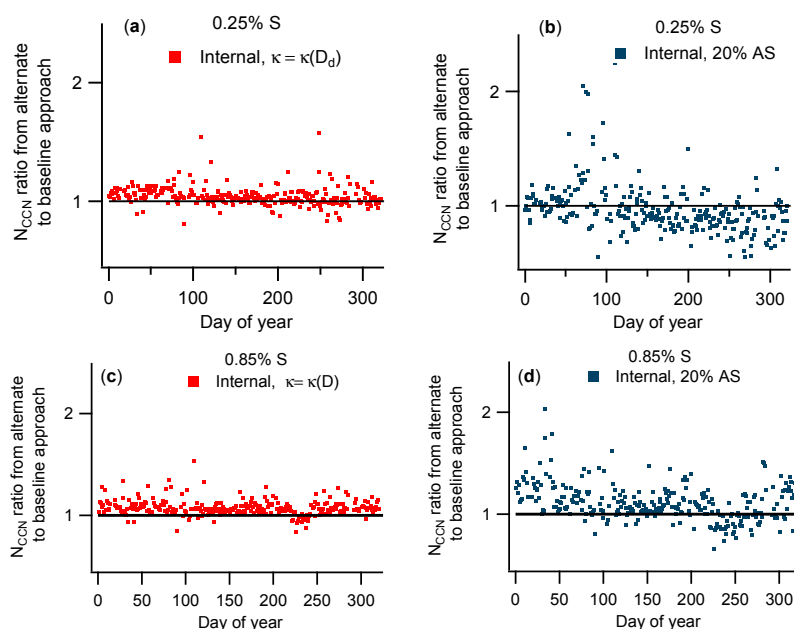

Figure 11. Time series for 2011 of estimated N_{CCN} relative to that from the baseline approach: (**a**) internal mixture, $\kappa = \kappa(D)$ at 0.25% S; (**b**) internal mixture, 20% AS at 0.25% S (**c**) internal mixture, $\kappa = \kappa(D)$ at 0.85% S; and (**d**) internal mixture, 20% AS at 0.85% S.

4. Summary and Conclusions

Size distributions and hygroscopic growth factor distributions measured from 2009 to 2012 at the SGP ARM site were used to estimate CCN concentrations over a range in supersaturation. An initial estimate of N_{CCN} that served as a basis for comparison used all of the information in the combined distributions without any averaging. For those estimates, matrices of $N(D_d, \kappa)$ and $S_c(D_d, \kappa)$ were calculated from the measured distributions and from κ-Köhler Theory, respectively, and $N_{CCN}(S)$ was calculated by integrating all of the N elements for which the corresponding S_c element < S. Comparisons of those estimates with direct measurements from a collocated CCN counter show that this baseline approach can reasonably predict N_{CCN} over a range of S.

The baseline spectra were then compared with those calculated using the same dataset but with aerosol treatments that are more commonly used for more efficient computation or simply

because size-dependent composition or hygroscopicity distributions are not available. These included approximating the aerosol as an internal mixture with fixed inorganic volume fraction, as an internal mixture with size-dependent or size-independent hygroscopicity, and as an external mixture with size-dependent or size-independent hygroscopicity. Bias and variance relative to the baseline estimates were described with best fit slopes, *m*, and coefficients of determination, r^2, respectively, with both calculated from the thousands of N_{CCN} pairs over the period of analysis.

Though the results presented here are most directly applicable for the aerosol at SGP, that aerosol is quite diverse, with a range in sources, origins, and atmospheric processing prior to sampling. Thus, at least the overall ~10% uncertainty range accompanying assumption of either internal or external mixtures reported here is likely relevant for N_{CCN} prediction in other regions as well and can provide some guidance for interpretation of model results. And for prediction of N_{CCN} for an aerosol known to be similar to that at SGP the bias and scatter associated with each of the simplified treatments can be weighed together with computational cost for selection of the most appropriate approximation(s). Ongoing work is aimed at applying these results to improve the accuracy with which CCN spectra at SGP and other ARM sites can be predicted in the absence of direct measurements.

References

1. Köhler, H. The nucleus in and the growth of hygroscopic droplets. *Trans. Faraday Soc.* **1936**, *32*, 1152–1161. [CrossRef]
2. Hallquist, M.; Wenger, J.C.; Baltensperger, U.; Rudich, Y.; Simpson, D.; Claeys, M.; Dommen, J.; Donahue, N.M.; George, C.; Goldstein, A.H.; et al. The formation, properties and impact of secondary organic aerosol: Current and emerging issues. *Atmos. Chem. Phys.* **2009**, *9*, 5155–5236. [CrossRef]
3. Pennington, M.R.; Bzdek, B.R.; Depalma, J.W.; Smith, J.N.; Kortelainen, A.-M.; Ruiz, L.H.; Petäjä, T.; Kulmala, M.; Worsnop, D.R.; Johnston, M.V. Identification and quantification of particle growth channels during new particle formation. *Atmos. Chem. Phys.* **2013**, *13*, 10215–10225. [CrossRef]
4. Abbatt, J.; Broekhuizen, K.; Pradeepkumar, P. Cloud condensation nucleus activity of internally mixed ammonium sulfate/organic acid aerosol particles. *Atmos. Environ.* **2005**, *39*, 4767–4778. [CrossRef]
5. Prenni, A.J.; Petters, M.D.; Kreidenweis, S.M.; Demott, P.J.; Ziemann, P.J. Cloud droplet activation of secondary organic aerosol. *J. Geophys. Res.* **2007**, *112*. [CrossRef]
6. Bigg, E. Discrepancy between observation and prediction of concentrations of cloud condensation nuclei. *Atmos. Res.* **1986**, *20*, 81–86. [CrossRef]
7. Chan, M.N.; Kreidenweis, S.M.; Chan, C.K. Measurements of the Hygroscopic and Deliquescence Properties of Organic Compounds of Different Solubilities in Water and Their Relationship with Cloud Condensation Nuclei Activities. *Environ. Sci. Technol.* **2008**, *42*, 3602–3608. [CrossRef] [PubMed]
8. Raymond, T.M. Cloud activation of single-component organic aerosol particles. *J. Geophys. Res.* **2002**, *107*. [CrossRef]
9. Raymond, T.M. Formation of cloud droplets by multicomponent organic particles. *J. Geophys. Res.* **2003**, *108*. [CrossRef]
10. Roberts, G.C. Sensitivity of CCN spectra on chemical and physical properties of aerosol: A case study from the Amazon Basin. *J. Geophys. Res.* **2002**, *107*. [CrossRef]

11. Smith, J.N.; Dunn, M.J.; Vanreken, T.M.; Iida, K.; Stolzenburg, M.R.; Mcmurry, P.H.; Huey, L.G. Chemical composition of atmospheric nanoparticles formed from nucleation in Tecamac, Mexico: Evidence for an important role for organic species in nanoparticle growth. *Geophys. Res. Lett.* **2008**, *35*. [CrossRef]

12. Yli-Juuti, T.; Nieminen, T.; Hirsikko, A.; Aalto, P.P.; Asmi, E.; Hõrrak, U.; Manninen, H.E.; Patokoski, J.; Maso, M.D.; Petäjä, T.; et al. Growth rates of nucleation mode particles in Hyytiälä during 2003−2009: Variation with particle size, season, data analysis method and ambient conditions. *Atmos. Chem. Phys.* **2011**, *11*, 12865–12886. [CrossRef]

13. Ruehl, C.R.; Davis, J.F.; Wilson, K.R. An interfacial mechanism for cloud droplet formation on organic aerosols. *Science* **2016**, *351*, 1447–1450. [CrossRef] [PubMed]

14. Bilde, M.; Svenningsson, B. CCN activation of slightly soluble organics: The importance of small amounts of inorganic salt and particle phase. *Tellus* **2004**, *56*, 128–134. [CrossRef]

15. Hartz, K.E.H.; Tischuk, J.E.; Chan, M.N.; Chan, C.K.; Donahue, N.M.; Pandis, S.N. Cloud condensation nuclei activation of limited solubility organic aerosol. *Atmos. Environ.* **2006**, *40*, 605–617. [CrossRef]

16. Svenningsson, B.; Rissler, J.; Swietlicki, E.; Mircea, M.; Bilde, M.; Facchini, M.C.; Decesari, S.; Fuzzi, S.; Zhou, J.; Mønster, J.; Rosenørn, T. Hygroscopic growth and critical supersaturations for mixed aerosol particles of inorganic and organic compounds of atmospheric relevance. *Atmos. Chem. Phys.* **2006**, *6*, 1937–1952. [CrossRef]

17. Petters, M.D.; Kreidenweis, S.M. A single parameter representation of hygroscopic growth and cloud condensation nucleus activity. *Atmos. Chem. Phys.* **2007**, *7*, 1961–1971. [CrossRef]

18. Moore, R.H.; Bahreini, R.; Brock, C.A.; Froyd, K.D.; Cozic, J.; Holloway, J.S.; Middlebrook, A.M.; Murphy, D.M.; Nenes, A. Hygroscopicity and composition of Alaskan Arctic CCN during April 2008. *Atmos. Chem. Phys.* **2011**, *11*, 11807–11825. [CrossRef]

19. Bougiatioti, A.; Fountoukis, C.; Kalivitis, N.; Pandis, S.N.; Nenes, A.; Mihalopoulos, N. Cloud condensation nuclei measurements in the marine boundary layer of the Eastern Mediterranean: CCN closure and droplet growth kinetics. *Atmos. Chem. Phys.* **2009**, *9*, 7053–7066. [CrossRef]

20. Chang, R.Y.-W.; Slowik, J.G.; Shantz, N.C.; Vlasenko, A.; Liggio, J.; Sjostedt, S.J.; Leaitch, W.R.; Abbatt, J.P.D. The hygroscopicity parameter (κ) of ambient organic aerosol at a field site subject to biogenic and anthropogenic influences: Relationship to degree of aerosol oxidation. *Atmos. Chem. Phys.* **2010**, *10*, 5047–5064. [CrossRef]

21. Chuang, P.Y.; Collins, D.R.; Pawlowska, H.; Snider, J.R.; Jonsson, H.H.; Brenguier, J.L.; Flagan, R.C.; Seinfeld, J.H. CCN measurements during ACE-2 and their relationship to cloud microphysical properties. *Tellus* **2000**, *52*, 843–867. [CrossRef]

22. Covert, D.S.; Gras, J.L.; Wiedensohler, A.; Stratmann, F. Comparison of directly measured CCN with CCN modeled from the number-size distribution in the marine boundary layer during ACE 1 at Cape Grim, Tasmania. *J. Geophys. Res. Atmos.* **1998**, *103*, 16597–16608. [CrossRef]

23. Furutani, H.; Dallosto, M.; Roberts, G.; Prather, K. Assessment of the relative importance of atmospheric aging on CCN activity derived from field observations. *Atmos. Environ.* **2008**, *42*, 3130–3142. [CrossRef]

24. Gácita, M.S.; Longo, K.M.; Freire, J.L.M.; Freitas, S.R.; Martin, S.T. Impact of mixing state and hygroscopicity on CCN activity of biomass burning aerosol in Amazonia. *Atmos. Chem. Phys.* **2017**, *17*, 2373–2392. [CrossRef]

25. Kammermann, L.; Gysel, M.; Weingartner, E.; Herich, H.; Cziczo, D.J.; Holst, T.; Svenningsson, B.; Arneth, A.; Baltensperger, U. Subarctic atmospheric aerosol composition: 3. Measured and modeled properties of cloud condensation nuclei. *J. Geophys. Res.* **2010**, *115*. [CrossRef]

26. Kuwata, M.; Kondo, Y.; Miyazaki, Y.; Komazaki, Y.; Kim, J.H.; Yum, S.S.; Tanimoto, H.; Matsueda, H. Cloud condensation nuclei activity at Jeju Island, Korea in spring 2005. *Atmos. Chem. Phys.* **2008**, *8*, 2933–2948. [CrossRef]

27. Mircea, M.; Facchini, M.C.; Decesari, S.; Fuzzi, S.; Charlson, R.J. The influence of the organic aerosol component on CCN supersaturation spectra for different aerosol types. *Tellus* **2002**, *54*, 74–81. [CrossRef]

28. Moore, R.H.; Cerully, K.; Bahreini, R.; Brock, C.A.; Middlebrook, A.M.; Nenes, A. Hygroscopicity and composition of California CCN during summer 2010. *J. Geophys. Res. Atmos.* **2012**, *117*. [CrossRef]

29. Rissler, J.; Vestin, A.; Swietlicki, E.; Fisch, G.; Zhou, J.; Artaxo, P.; Andreae, M.O. Size distribution and hygroscopic properties of aerosol particles from dry-season biomass burning in Amazonia. *Atmos. Chem. Phys.* **2006**, *6*, 471–491. [CrossRef]

30. Roberts, G.C.; Day, D.A.; Russell, L.M.; Dunlea, E.J.; Jimenez, J.L.; Tomlinson, J.M.; Collins, D.R.; Shinozuka, Y.; Clarke, A.D. Characterization of particle cloud droplet activity and composition in the free troposphere and the boundary layer during INTEX-B. *Atmos. Chem. Phys.* **2010**, *10*, 6627–6644. [CrossRef]

31. Roberts, G.; Mauger, G.; Hadley, O.; Ramanathan, V. North American and Asian aerosols over the eastern Pacific Ocean and their role in regulating cloud condensation nuclei. *J. Geophys. Res.* **2006**, *111*. [CrossRef]

32. Rose, D.; Nowak, A.; Achtert, P.; Wiedensohler, A.; Hu, M.; Shao, M.; Zhang, Y.; Andreae, M.O.; Pöschl, U. Cloud condensation nuclei in polluted air and biomass burning smoke near the mega-city Guangzhou, China—Part 1: Size-resolved measurements and implications for the modeling of aerosol particle hygroscopicity and CCN activity. *Atmos. Chem. Phys.* **2010**, *10*, 3365–3383. [CrossRef]

33. Shantz, N.C.; Leaitch, W.R.; Phinney, L.; Mozurkewich, M.; Toom-Sauntry, D. The effect of organic compounds on the growth rate of cloud droplets in marine and forest settings. *Atmos. Chem. Phys.* **2008**, *8*, 5869–5887. [CrossRef]

34. Wang, J.; Cubison, M.J.; Aiken, A.C.; Jimenez, J.L.; Collins, D.R. The importance of aerosol mixing state and size-resolved composition on CCN concentration and the variation of the importance with atmospheric aging of aerosols. *Atmos. Chem. Phys.* **2010**, *10*, 7267–7283. [CrossRef]

35. Ervens, B.; Cubison, M.J.; Andrews, E.; Feingold, G.; Ogren, J.A.; Jimenez, J.L.; Quinn, P.K.; Bates, T.S.; Wang, J.; Zhang, Q.; et al. CCN predictions using simplified assumptions of organic aerosol composition and mixing state: A synthesis from six different locations. *Atmos. Chem. Phys.* **2010**, *10*, 4795–4807. [CrossRef]

36. Broekhuizen, K.; Chang, R.-W.; Leaitch, W.R.; Li, S.-M.; Abbatt, J.P.D. Closure between measured and modeled cloud condensation nuclei (CCN) using size-resolved aerosol compositions in downtown Toronto. *Atmos. Chem. Phys.* **2006**, *6*, 2513–2524. [CrossRef]

37. Cubison, M.J.; Ervens, B.; Feingold, G.; Docherty, K.S.; Ulbrich, I.M.; Shields, L.; Prather, K.; Hering, S.; Jimenez, J.L. The influence of chemical composition and mixing state of Los Angeles urban aerosol on CCN number and cloud properties. *Atmos. Chem. Phys.* **2008**, *8*, 5649–5667. [CrossRef]

38. Lance, S.; Nenes, A.; Mazzoleni, C.; Dubey, M.K.; Gates, H.; Varutbangkul, V.; Rissman, T.A.; Murphy, S.M.; Sorooshian, A.; Flagan, R.C.; et al. Cloud condensation nuclei activity, closure, and droplet growth kinetics of Houston aerosol during the Gulf of Mexico Atmospheric Composition and Climate Study (GoMACCS). *J. Geophys. Res.* **2009**, *114*. [CrossRef]

39. Padró, L.T.; Moore, R.H.; Zhang, X.; Rastogi, N.; Weber, R.J.; Nenes, A. Mixing state and compositional effects on CCN activity and droplet growth kinetics of size-resolved CCN in an urban environment. *Atmos. Chem. Phys.* **2012**, *12*, 10239–10255. [CrossRef]

40. Zaveri, R.A.; Barnard, J.C.; Easter, R.C.; Riemer, N.; West, M. Particle-resolved simulation of aerosol size, composition, mixing state, and the associated optical and cloud condensation nuclei activation properties in an evolving urban plume. *J. Geophys. Res.* **2010**, *115*. [CrossRef]

41. Bhattu, D.; Tripathi, S.N. CCN closure study: Effects of aerosol chemical composition and mixing state. *J. Geophys. Res. Atmos.* **2015**, *120*, 766–783. [CrossRef]

42. Gunthe, S.S.; King, S.M.; Rose, D.; Chen, Q.; Roldin, P.; Farmer, D.K.; Jimenez, J.L.; Artaxo, P.; Andreae, M.O.; Martin, S.T.; et al. Cloud condensation nuclei in pristine tropical rainforest air of Amazonia: Size-resolved measurements and modeling of atmospheric aerosol composition and CCN activity. *Atmos. Chem. Phys.* **2009**, *9*, 7551–7575. [CrossRef]

43. Medina, J.; Nenes, A.; Sotiropoulou, R.-E.P.; Cottrell, L.D.; Ziemba, L.D.; Beckman, P.J.; Griffin, R.J. Cloud condensation nuclei closure during the International Consortium for Atmospheric Research on Transport and Transformation 2004 campaign: Effects of size-resolved composition. *J. Geophys. Res.* **2007**, *112*. [CrossRef]

44. Stroud, C.A.; Nenes, A.; Jimenez, J.L.; Decarlo, P.F.; Huffman, J.A.; Bruintjes, R.; Nemitz, E.; Delia, A.E.; Toohey, D.W.; Guenther, A.B.; et al. Cloud Activating Properties of Aerosol Observed during CELTIC. *J. Atmos. Sci.* **2007**, *64*, 441–459. [CrossRef]

45. Conant, W.C.; Vanreken, T.M.; Rissman, T.A.; Varutbangkul, V.; Jonsson, H.H.; Nenes, A.; Jimenez, J.L.; Delia, A.E.; Bahreini, R.; Roberts, G.C.; et al. Aerosol-cloud drop concentration closure in warm cumulus. *J. Geophys. Res. Atmos.* **2004**, *109*. [CrossRef]

46. Dusek, U.; Frank, G.P.; Hildebrandt, L.; Curtius, J.; Schneider, J.; Walter, S.; Chand, D.; Drewnick, F.; Hings, S.; Jung, D.; et al. Size Matters More Than Chemistry for Cloud-Nucleating Ability of Aerosol Particles. *Science* **2006**, *312*, 1375–1378. [CrossRef] [PubMed]

47. Cantrell, W.; Shaw, G.; Cass, G.R.; Chowdhury, Z.; Hughes, L.S.; Prather, K.A.; Guazzotti, S.A.; Coffee, K.R. Closure between aerosol particles and cloud condensation nuclei at Kaashidhoo Climate Observatory. *J. Geophys. Res. Atmos.* **2001**, *106*, 28711–28718. [CrossRef]

48. Chang, R.-W.; Liu, P.; Leaitch, W.; Abbatt, J. Comparison between measured and predicted CCN concentrations at Egbert, Ontario: Focus on the organic aerosol fraction at a semi-rural site. *Atmos. Environ.* **2007**, *41*, 8172–8182. [CrossRef]

49. Liu, P.S.K.; Leaitch, W.R.; Banic, C.M.; Li, S.-M.; Ngo, D.; Megaw, W.J. Aerosol observations at Chebogue Point during the 1993 North Atlantic Regional Experiment: Relationships among cloud condensation nuclei, size distribution, and chemistry. *J. Geophys. Res. Atmos.* **1996**, *101*, 28971–28990. [CrossRef]

50. Rissler, J.; Swietlicki, E.; Zhou, J.; Roberts, G.; Andreae, M.O.; Gatti, L.V.; Artaxo, P. Physical properties of the sub-micrometer aerosol over the Amazon rain forest during the wet-to-dry season transition—Comparison of modeled and measured CCN concentrations. *Atmos. Chem. Phys.* **2004**, *4*, 2119–2143. [CrossRef]

51. Vanreken, T.M. Toward aerosol/cloud condensation nuclei (CCN) closure during CRYSTAL-FACE. *J. Geophys. Res.* **2003**, *108*. [CrossRef]

52. Wang, J.; Lee, Y.-N.; Daum, P.H.; Jayne, J.; Alexander, M.L. Effects of aerosol organics on cloud condensation nucleus (CCN) concentration and first indirect aerosol effect. *Atmos. Chem. Phys.* **2008**, *8*, 6325–6339. [CrossRef]

53. Ervens, B.; Cubison, M.; Andrews, E.; Feingold, G.; Ogren, J.A.; Jimenez, J.L.; Decarlo, P.; Nenes, A. Prediction of cloud condensation nucleus number concentration using measurements of aerosol size distributions and composition and light scattering enhancement due to humidity. *J. Geophys. Res.* **2007**, *112*. [CrossRef]

54. Almeida, G.P.; Brito, J.; Morales, C.A.; Andrade, M.F.; Artaxo, P. Measured and modelled cloud condensation nuclei (CCN) concentration in São Paulo, Brazil: The importance of aerosol size-resolved chemical composition on CCN concentration prediction. *Atmos. Chem. Phys.* **2014**, *14*, 7559–7572. [CrossRef]

55. Asa-Awuku, A.; Moore, R.H.; Nenes, A.; Bahreini, R.; Holloway, J.S.; Brock, C.A.; Middlebrook, A.M.; Ryerson, T.B.; Jimenez, J.L.; Decarlo, P.F.; et al. Airborne cloud condensation nuclei measurements during the 2006 Texas Air Quality Study. *J. Geophys. Res.* **2011**, *116*. [CrossRef]

56. Che, H.C.; Zhang, X.Y.; Wang, Y.Q.; Zhang, L.; Shen, X.J.; Zhang, Y.M.; Ma, Q.L.; Sun, J.Y.; Zhang, Y.W.; Wang, T.T. Characterization and parameterization of aerosol cloud condensation nuclei activation under different pollution conditions. *Sci. Rep.* **2016**, *6*. [CrossRef] [PubMed]

57. Mircea, M.; Facchini, M.C.; Decesari, S.; Cavalli, F.; Emblico, L.; Fuzzi, S.; Vestin, A.; Rissler, J.; Swietlicki, E.; Frank, G.; et al. Importance of the organic aerosol fraction for modeling aerosol hygroscopic growth and activation: A case study in the Amazon Basin. *Atmos. Chem. Phys.* **2005**, *5*, 3111–3126. [CrossRef]

58. Quinn, P.K.; Bates, T.S.; Coffman, D.J.; Covert, D.S. Influence of particle size and chemistry on the cloud nucleating properties of aerosols. *Atmos. Chem. Phys.* **2008**, *8*, 1029–1042. [CrossRef]

59. Mahish, M.; Collins, D. Analysis of a Multi-Year Record of Size-Resolved Hygroscopicity Measurements from a Rural Site in the U.S. *Aerosol Air Qual. Res.* **2017**, *17*, 1389–1400. [CrossRef]

60. Collins, D. *Tandem Differential Mobility Analyzer/Aerodynamic Particle Sizer (APS) Handbook*; No. DOE/SC-ARM-TR-090; U.S. Department of Energy: Washington, DC, USA, 2010.

61. Gasparini, R.; Li, R.; Collins, D.R. Integration of size distributions and size-resolved hygroscopicity measured during the Houston Supersite for compositional categorization of the aerosol. *Atmos. Environ.* **2004**, *38*, 3285–3303. [CrossRef]

62. Roberts, G.; Nenes, A. A Continuous-Flow Streamwise Thermal-Gradient CCN Chamber for Atmospheric Measurements. *Aerosol Sci. Technol.* **2005**, *39*, 206–221. [CrossRef]

63. Jefferson, A. *Aerosol Observing System (AOS) Handbook*; Technical Report ARM-TR-014; U.S. Department of Energy: Washington, DC, USA, 2011.

64. Ng, N.L.; Herndon, S.C.; Trimborn, A.; Canagaratna, M.R.; Croteau, P.L.; Onasch, T.B. An Aerosol Chemical Speciation Monitor (ACSM) for Routine Monitoring of the Composition and Mass Concentrations of Ambient Aerosol. *Aerosol Sci. Technol.* **2011**, *45*, 780–794. [CrossRef]

65. Bond, T.C.; Anderson, T.L.; Campbell, D. Calibration and intercomparison of filter-based measurements of visible light absorption by aerosols. *Aerosol Sci. Technol.* **1999**, *30*, 582–600. [CrossRef]

66. Watson, T.B. *Aerosol Chemical Speciation Monitor (ACSM) Instrument Handbook*; No. DOE/SC-ARM-TR-196; U.S. Department of Energy: Washington, DC, USA, 2017.

67.　Yang, M.; Howell, S.G.; Zhuang, J.; Huebert, B.J. Attribution of aerosol light absorption to black carbon, brown carbon, and dust in China—Interpretations of atmospheric measurements during EAST-AIRE. *Atmos. Chem. Phys.* **2009**, *9*, 2035–2050. [CrossRef]

68.　Nakao, S.; Tang, P.; Tang, X.; Clark, C.H.; Qi, L.; Seo, E.; Asa-Awuku, A.; Cocker, D. Density and elemental ratios of secondary organic aerosol: Application of a density prediction method. *Atmos. Environ.* **2013**, *68*, 273–277. [CrossRef]

69.　Fast, J.; Zhang, Q.; Tilp, A.; Shippert, T.; Parworth, C.; Mei, F. *Organic Aerosol Component (OACOMP) Value-Added Product*; No. DOE/SC-ARM-TR-131; U.S. Department of Energy: Washington, DC, USA, 2013.